Computational Fluid Dynamics-Based Design of Finned Steam Cracking Reactors

Carl M. Schietekat, David J. Van Cauwenberge, Kevin M. Van Geem, and Guy B. Marin
Laboratory for Chemical Technology, Dept. of Chemical Technology, Ghent University, Gent 9052, Belgium

DOI 10.1002/aic.14326
Published online December 27, 2013 in Wiley Online Library (wileyonlinelibrary.com)

The use of one-dimensional reactor models to simulate industrial steam cracking reactors has been one of the main limiting factors for the development of new reactor designs and the evaluation of existing three-dimensional (3-D) reactor configurations. Therefore, a 3-D computational fluid dynamics approach is proposed in which the detailed free-radical chemistry is for the first time accounted for. As a demonstration case, the application of longitudinally and helicoidally finned tubes as steam cracking reactors was investigated under industrially relevant conditions. After experimental validation of the modeling approach, a comprehensive parametric study allowed to identify optimal values of the fin parameters, that is, fin height, number of fins, and helix angle to maximize heat transfer. Reactive simulations of an industrial Millisecond propane cracker were performed for four distinct finned reactors using a reaction network of 26 species and 203 elementary reactions. The start-of-run tube metal skin temperatures could be reduced by up to 50 K compared to conventionally applied tubular reactors when applying optimal fin parameters. Implementation of a validated coking model for light feedstocks shows that coking rates are reduced up to 50%. However, the increased friction and inner surface area lead to pressure drops higher by a factor from 1.22 to 1.66 causing minor but significant shifts in light olefin selectivity. For the optimized helicoidally finned reactor the ethene selectivity dropped, whereas propene and 1,3-butadiene selectivity increased with a similar amount. The presented methodology can be applied in a straightforward way to other 3-D reactor designs and can be extended to more complex feedstocks such as naphtha. © 2013 American Institute of Chemical Engineers *AIChE J*, 60: 794–808, 2014

Keywords: steam cracking, computational fluid dynamics, olefins, coke formation, finned reactor, enhanced heat transfer

Introduction

Steam cracking of hydrocarbons is the predominant commercial process for producing many platform chemicals such as light olefins (i.e., ethene, propene, and butadiene) and aromatics (i.e., benzene, toluene, and xylenes). These platform chemicals are the building blocks for most polymers and the starting molecules for the production of many additives, solvents, and other high-value chemicals. The process is one of the most energy-intensive processes in the chemical industry using about 8% of the industry's primary energy consumption.[1] This is mainly associated with the energy consumed in the separation section, in which temperatures lower than 160 K can be encountered.[2] However, also in the furnace considerable energy efficiency improvements are possible. Per ton high-value chemicals approximately 1 ton of CO_2 is produced and depending on the cracker's design and feedstock 10–15 GJ energy is consumed.[1,3] A major factor for the process energy efficiency is the formation of coke on the inner wall of the tubular cracking reactors. This carbonaceous coke layer reduces the cross-sectional area and leads to an increasing reactor pressure drop over time. The latter promotes bimolecular reactions over monomolecular reactions, resulting in a loss of olefin selectivity.[4] Moreover, this coke layer is highly insulating, increasing the conductive resistance for heat transfer from the furnace to the process gas. To maintain the same cracking severity, this increased heat-transfer resistance is compensated by increasing the fuel input to the furnace burners. This leads to higher reactor tube skin temperatures (TMT). Eventually, either metallurgical constraints of the reactor alloy or an excessive pressure drop over the reactor will force the operators to cease production and decoke the reactors. Typically, this will require production to be halted for 48 h, having a considerable adverse effect on the economics of the process.

In light of this energetic and economic drawback, many efforts have been made toward the development of technologies to reduce coke formation. These technologies can be divided in three groups: the use of additives, the use of surface technologies, and three-dimensional (3-D) reactor configurations for heat-transfer enhancement. As additives, mainly sulfur containing components[5] are used. Although a general consensus exists on the beneficial effect for the suppression of CO production, the reported effect on coke formation is contradictory.[6,7] For metal surface technologies, low-coking alloys[8] and (catalytic) coatings[9–12] are typically studied.

Correspondence concerning this article should be addressed to K. M. Van Geem at Kevin.VanGeem@UGent.be.

In this work, the focus is on the third group, that is, the application of 3-D reactor configurations. By means of improved heat transfer, lower temperatures at the coke-gas interface, and thus lower coking rates are obtained compared to conventional tubular reactors. Alternatively, the reactor throughput and the furnace fuel flow rate could be increased while maintaining the TMT. One such 3-D reactor configuration is the use of longitudinal or helicoidal fins on the reactor tube inner surface, allowing improved heat transfer mainly because of an increased internal surface area.

Although the literature on this topic for heat exchanger applications is extensive,[13–15] the characteristics of the flow inside finned tubes are still not well understood due to the limited availability of accurate experimental data.[15] Water flow visualization studies indicate the existence of different regimes, depending on the angle between the fins and the tube axis.[14,16] For helix angles smaller than 30° and for relatively tall and few fins, a rotational pattern dominates as the flow follows the space in between the fins and swirling flow, that is, flow with a large azimuthal velocity component, is established. However, when using larger helix angles the flow is seen to be prone to coring, that is, the main portion of the flow is constrained to the core of the tube, with possible relaminarization between the fins. A number of correlations for the Nusselt numbers and friction factors of these tubes have already been proposed, but none of these are valid over the entire range of fin dimensions and Reynolds numbers.[15]

Although in heat exchangers a wide variety of fin shapes is used, the fins typically applied in pyrolysis reactors are rounded fins with a smooth concave–convex structure in order to avoid flow separation and possible local hot spots for coke formation. Figure 1 shows the cross section of the adopted tubes. The geometric parameters are the tube outer diameter OD, the maximum inner diameter D, the fin height e, the minimum metal thickness t, and the fin width w. The curvature of the fins is determined by two touching circles as shown in dashed lines in Figure 1. Only four parameters can be chosen independently. Typically, the tube outer and maximum inner diameter, the fin height, and the number of fins are chosen. In longitudinally finned tubes, the cross section is extruded along the tube centerline, that is, the fins are parallel to the tube centerline. In helicoidally finned tubes, the fins are extruded along a helix. Hence, for helicoidally finned tubes an additional geometric parameter can be chosen, that is, the helix angle. This helix angle corresponds to the angle between the helicoidal fins and the tube centerline.

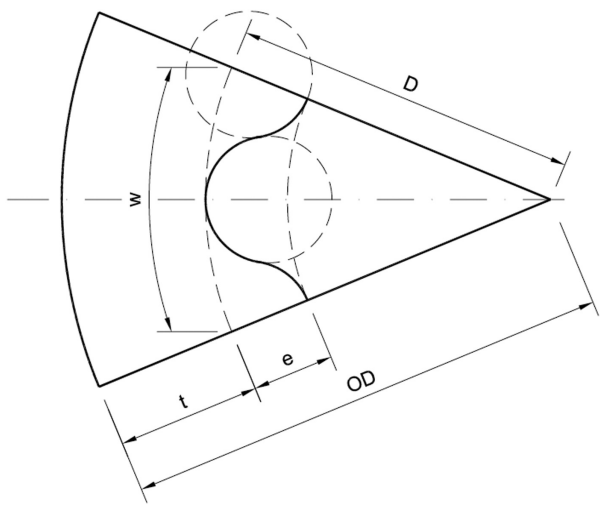

Figure 1. Part of the cross-section of a finned tube; OD: outer diameter, *D*: inner diameter, *w*: fin width, *e*: fin height, and *t*: minimum metal thickness.

A study by Brown on these geometries indicated that the heat transfer improvement for longitudinally finned tubes follows a linear relationship with the surface area increase.[17] Albano et al. compared a longitudinally and helicoidally finned tube by performing air flow experiments through a heated tube.[18] The Colburn j-factors for the longitudinally and helicoidally finned tubes were found to be, respectively, 20 and 40% lower than for bare tubes. However, this loss was offset by a 44% increase in internal surface area compared to an equivalent bare tube, that is, a bare tube with the same cross-sectional surface area. The better performance of the longitudinally finned compared to the helicoidally finned tubes was attributed to a greater tendency of the air to bypass the fins in the latter. Pressure drops were measured to be higher for the helicoidally finned tubes compared to longitudinally finned tubes. The latter was confirmed by the simulation results obtained by De Saegher et al.[19] for an industrial propane cracking reactor. In contrast to Albano et al., these authors simulated a higher heat-transfer coefficient for the helicoidally finned tube compared to the corresponding longitudinally finned tube. This was attributed to more intense mixing and reduced radial temperature gradients in the helicoidally finned tubes. The accuracy of the results of De Saegher et al.[19] can be debated because of the adopted coarse computational grid and the first-order discretization schemes that were used due to much lower computational capabilities. A recent patent by Higuchi et al.[20] covers a slightly different geometry where the fins cover only part of the tube perimeter with bare spaces in-between. Based on computational fluid dynamics (CFD) simulations of air flow, favorable ranges for the fin dimensions were determined. The optimal helix angle was found to be around 25–30°, whereas the optimal fin height-to-diameter ratio was determined to be between 0.1 and 0.2. Increasing the fin height-to-width ratio was found to be favorable as more intense heating was achieved. An upper limit of 0.7 was determined based on the limitations of the fin welding process and practical implications, for example, plugging of the reactor during decoking operation by spalled cokes. Wolpert et al.[21] also recently proposed helicoidally finned tubes with a lower fin height than the aforementioned references. The authors state that this allows the generation of swirling flow in the immediate vicinity of the fins and that this swirling flow spreads to the tube core.

The above clearly shows that in order to properly assess the full potential of finned reactors, the influence of each of the geometric parameters needs to be investigated systematically. To the authors' knowledge, this has not been done before. More importantly the availability of a reliable simulation model for 3-D reactor geometries in which the free-radical gas-phase chemistry is accounted for next to coke formation and fluid dynamics would open the door for a more rapid evaluation of new and existing 3-D reactor designs. Although many efforts have been made toward the accurate CFD simulation of the fire-side of steam cracking units,[22–31] the literature on CFD simulations of the reactor-side is limited.[19,27,28,31] Besides the work of De Saegher

et al.,[19] all aforementioned references use highly simplified global reaction networks. Only detailed free-radical reaction networks capture the essential chemistry to allow a trustworthy prediction of the effect of reactor configuration on product yields. As mentioned before the simulations of De Saegher et al.[19] were performed on a coarse computational grid and adopted first-order discretization schemes. To the authors' knowledge, no grid-independent simulations of steam cracking reactors with higher-order discretization schemes and a free-radical reaction network have been published. Therefore, in this work, the Reynolds-averaged Navier–Stokes approach is combined with such a detailed single-event microkinetic model. The first step is the validation of the CFD model using available experimental data. Second, the potential of the application of internally finned tubes in steam crackers is assessed by performing a comprehensive nonreactive parametric CFD study providing guidelines for optimal design. Finally, optimal designs are evaluated in an industrial propane cracking Millisecond furnace. The effect of the selected 3-D reactor geometries on product selectivities and coking tendency is evaluated. The results are validated with industrial data from a Millisecond furnace operated under similar conditions.

CFD Model Set-Up

Governing equations

For a steady-state 3-D simulation of compressible reactive gas flow, the governing equations are the following

- Global continuity equation

$$\nabla(\rho\bar{u})=0 \tag{1}$$

- Navier–Stokes equations

$$\nabla\cdot(\rho\bar{u}\bar{u})=-\nabla p+\nabla\cdot\bar{\bar{\tau}} \tag{2}$$

- Energy equation

$$\nabla\cdot(\bar{u}(\rho E+p))=\nabla\cdot\left(k_{\text{eff}}\nabla T-\sum_i h_i\bar{J}_i\right)+S_{\text{h}} \tag{3}$$

- Species continuity equations

$$\nabla\cdot(\rho\bar{u}Y_i)=-\nabla\cdot\bar{J}_i+R_i\ ,\ \ \forall i=1,\text{nspec}-1 \tag{4}$$

In these equations $\bar{J}_i$ is the diffusion flux of species i, including contributions from both the laminar and turbulent diffusivity as well as the thermal (Soret) diffusivity. S_{h} is the heat of reaction, Y_i the mass fraction of species i, R_i the net rate of production of species i, and nspec the number of species. The performed simulations showed that in future work the laminar and thermal diffusivity do not need to be explicitly accounted for because the turbulent diffusion is always at least two orders of magnitude greater than the sum of both.

Turbulence modeling

The flow properties are Reynolds-decomposed to a steady mean value and a fluctuating turbulent contribution. This generates an additional stress tensor, characterizing the transfer of momentum by turbulence, the so-called Reynolds stresses: $\tau_{ij}^t=-\rho\overline{u_i'u_j'}$. Closure for these additional unknowns was provided by use of the Boussinesq approximation, expressing the Reynolds stresses in terms of the mean velocities. If the transport of momentum is assumed to be a diffusive process, an eddy viscosity can be introduced, analog to the molecular viscosity. One of the most widely applied models for determining this eddy viscosity is the standard k-ε model, where two additional transport equations are solved for the turbulent kinetic energy k and the energy dissipation rate ε, respectively. For swirling flow, results can be further improved by use of the k-ε renormalization group (RNG) model as an extra source term is introduced to the dissipation equation in regions with large strain rate. Although at the basis of some very successful models, the Boussinesq approximation assumes isotropic eddy viscosity. Abandoning this concept, the Reynolds stress model (RSM) solves six additional transport equations for each of the components of the symmetric Reynolds stress tensor, along with an equation for the energy dissipation rate. Given the strong coupling between these seven additional partial differential equations, this makes computation much more expensive. As the RSM can model flow characteristics resulting from anisotropy of the Reynolds stresses, more accurate results are to be expected in highly swirling flows.

In the present work, the k-ε RNG model was used for the bare tubes and for the tubes with longitudinal fins. For the more complex, swirling flow inside the helicoidally finned tubes the k-ε RNG model was used for initial convergence. In a second step, RSM was used because it gave a better agreement with the experimental validation data discussed in CFD Model Validation.

Boundary conditions

At the tube inlet the temperature, mass-flow rate, turbulence parameters k and ε, and the composition of the process gas were imposed. The turbulence parameters were calculated for a turbulence intensity of 8% and a characteristic length scale of 10% of the tube hydraulic diameter. At the outlet of the tube, a constant pressure boundary condition was set as the coil outlet pressure is a controlled process condition in an industrial steam cracker. All other variables were extrapolated from the integration field. The no-slip boundary condition was set at the tube inner walls. To apply this condition for highly turbulent flow, FLUENT's enhanced wall treatment was used to "bridge" the solution variables in the near-wall cells. This model combines a two-layer model with enhanced wall functions by blending linear and logarithmic laws-of-the-wall. Validity of the use of a two-layer model was ensured by placing computational cells within the viscous sublayer, with the near-wall cells satisfying the $y^+<1$ condition. The energy equation was solved by applying either an adiabatic, isothermal boundary, or imposed heat-flux condition to the tube outer walls.

Chemistry model

Steam cracking of hydrocarbons mainly proceeds through a free-radical mechanism, which is characterized by a vast number of species and reactions.[32–35] The incorporation of such detailed chemical networks is computationally expensive.[36] Hence, to limit computational cost, a network specifically geared at propane cracking was used by reducing the full single-event microkinetic CRACKSIM model[37–39] to its relevant core for propane cracking. The final network consisted of 203 reactions between 26 species, of which 13 radical species.

The Reaction Mechanism Generator (RMG) Transport estimator[40] was used for predicting the Lennard-Jones characteristic length and energy parameters.[41–54] These were then applied in FLUENT's kinetic theory method for calculation of thermal conductivity and viscosity for each individual species.[42,43] Diffusion coefficients were quantified on this basis as well by using a modification of the Chapman–Enskog formula.[44] Finally, thermal diffusion was taken into account by using an empirical composition-dependent form of the Soret diffusion coefficient.[45] Properties of the multicomponent mixture were calculated by ideal gas mixing laws.

Numerical model

The commercial CFD code ANSYS FLUENT 13.0 was adopted to solve the governing equations. This general-purpose CFD package uses the finite-volume method. Discretization of all equations was achieved using the quadratic upstream interpolation for convective kinetics scheme, combining the strengths of both upwind and central differencing schemes by using a three-point upstream quadratic interpolation. Although an unbounded scheme, it was selected based on the reported improved accuracy for rotating and swirling flows compared to the second-order up-wind scheme.[46] It can be proven that the scheme is third-order accurate.[46,47] The residual convergence criterion was set to 10^{-6} for all equations, only the energy and species equations were set lower to 10^{-9}. Furthermore the inlet pressure, outlet temperature, and species concentrations were monitored. The inlet pressure and outlet temperature were seen to change less than 1 Pa and 0.05 K, respectively, over the last 50 iterations for all simulations. The relative change over the last 50 iterations of all species concentrations was seen to change less than 0.1%.

Computational grid

The computational grid was constructed from a two-dimensional (2-D) triangular mesh which was extruded along the axial coordinate. For the helicoidally finned tubes, a twist vector was applied to obtain the correct helix angle. By symmetry considerations, the computational domain can be limited to one fin of the tube to reduce computational time. Periodic boundary conditions are applied to allow flow through the azimuthal boundaries in case of swirling flow. A fine boundary layer near the tube inner wall is added to ensure computational cells in the viscous sublayer having a $y^+ < 1$ as required by the enhanced wall treatment model. Grid independence for the tubes adopted by Albano et al.[18] was achieved at a mesh density of approximately 5.105 and 3.105 cells/m for the fluid and metal volume, respectively. Grid sizes in wall units[48] for grid independence were seen to be $\{R\Delta\theta^+,\ \Delta y^+,\ \Delta z^+\} = \{50,\ 0.8-50,\ 333\}$. These values were used as upper limits for all grids. These grids used in the reactive simulations were further refined based on the temperature gradient of the converged solution. The results of this grid refinement are shown in Supporting Information. No significant change in the results is seen by the grid refinement. The grid independent mesh for the tubes adopted by Albano et al.[18] is shown in Figure 2.

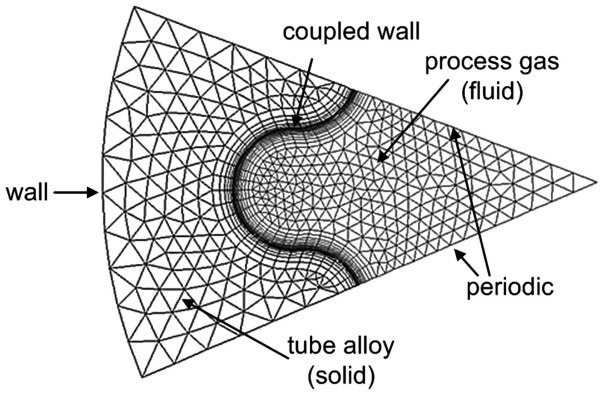

Figure 2. Grid independent mesh of a cross-section of the tubes adopted by Albano et al.[18]

CFD Model Validation

The CFD model was validated by comparison with the experimental results obtained by Albano et al.[18] By means of an experimental setup capable of measuring pressure drop and temperature along the axial coordinate, Albano et al. evaluated the heating performance of a longitudinally and a helicoidally finned tube. In their experimental setup, air flows through a steam-heated finned tube containing four thermocouples to measure the temperature in the center of the tube at different axial positions. As the air is being released to the atmosphere, the pressure at which the inlet diaphragm pump is operating indicates the pressure drop over the tube. For the exact dimensions of the tubes, reference is made to the original article of Albano et al.[18]

The experiments with a longitudinally and a helicoidally finned tube were performed at air mass-flow rates of 0.107 and 0.103 kg/s, respectively, which correspond to an inlet Reynolds number of approximately 230×10^3. It is important to stress that the experiments did not involve a sufficiently long inlet section to avoid entrance effects. In the performed CFD simulations, a small inlet section of 0.2-m length was included as the exact dimensions of the experimental inlet section are unknown. Furthermore, the temperatures measured on the outside of the tube were flawed due to steam condensation, leaving only the inner wall temperatures as reliable data. Hence, in the CFD simulations the inner wall temperature profile was imposed without taking conduction through the metal into account. The latter implies that the temperatures in the peaks and valleys were assumed to be equal, whereas in reality they differed by 1–2 K. Air was treated as an ideal gas with viscosity, specific heat capacity, and thermal conductivity following a piecewise-linear temperature dependence. The simulation results for pressure and temperature are compared to experimental data in Figure 3 for the longitudinally and helicoidally finned tube.

Pressure drops were simulated accurately with relative errors of 3.2 and 4.9% for the longitudinally and helicoidally finned tube, respectively. Temperatures were underpredicted for both tubes but it can be seen that the major difference lies in the entrance region. As the experimental setup did not include a sufficiently long adiabatic inlet section, the deviations near the inlet can be explained by the development of turbulent phenomena. Nevertheless, relative errors for the heat transfer were limited to 4.6 and 7.6%, which can be considered satisfactory given the experimental errors and the use of an azimuthally uniform internal wall temperature profile in the simulations.

Parametric Study

The validated CFD model was used to study the effect of the fin parameters on heat transfer and pressure drop through nonreactive air flow simulations. The dimensions studied are

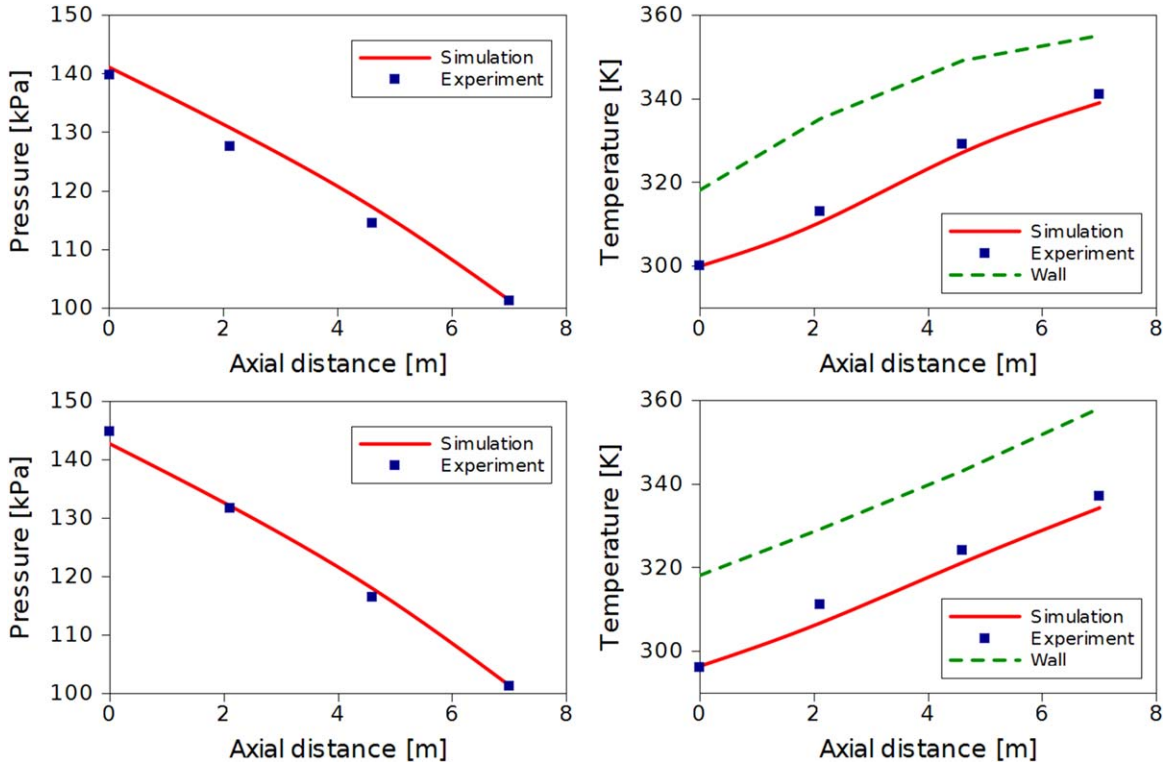

Figure 3. Pressure [kPa] (left) and temperature [K] (right) as function of axial position [m] in the longitudinally finned tube (top) at $Re = 233 \times 10^3$ and helicoidally finned tube (bottom) at $Re = 224 \times 10^3$; symbols, experimental values from Albano et al.[18]; ■; lines, simulated values; —.

[Color figure can be viewed in the online issue, which is available at wileyonlinelibrary.com.]

close to the typical ranges of patent and scientific literature.[18,21] However, the ranges studied in this work are broader than those discussed in previous studies.[18,21] The fins are distributed over the entire tube inner perimeter, that is, there are no locations without fins. The computational domain consisted of a 2-m long inlet section and a 4-m long test tube. The inlet section was an adiabatic tube and was used to provide fully developed flow at the test tube inlet. Both pressure-drop and temperature simulations were performed. In the former, the entire tube was simulated adiabatically, whereas in the latter the outer wall temperature was set to 373.15 K for the last 2 m of the test tube. The air inlet temperature was set to 300 K. This study was carried out at two flow rates (59.7 and 86.3 g/s), which corresponds to an inlet Reynolds numbers of 90×10^3 and 130×10^3, respectively, based on the equivalent diameter of the finned tubes, that is, the diameter of a bare tube with the same cross-sectional surface area, adopted by Albano et al.[18] The outlet pressure was set to 101,325 Pa as in the experiments performed by Albano et al.[18] In the following, results are given for the lowest inlet Reynolds number unless stated differently.

Heat transfer was quantified by calculating a heat-transfer coefficient based on the internal surface area of a bare tube with the same equivalent inner diameter. This heat-transfer coefficient was calculated based on the inlet and outlet temperatures, from which the amount of energy absorbed by the air can be calculated as follows

$$Q_{\text{abs}} = \phi_m c_P \left(T_{g,\text{out}} - T_{g,\text{in}}\right) \tag{5}$$

This same amount of absorbed energy can also be estimated in heat transfer terms as

$$Q_{\text{abs}} = \pi \; d_{\text{eq}} L_{\text{h}} U \; \text{LMTD} \tag{6}$$

By combination of Eqs. 5 and 6, the global heat-transfer coefficient based on the internal surface area of an equivalent bare tube can be expressed as

$$U = \frac{\phi_m \; c_P \left(T_{g,\text{out}} - T_{g,\text{in}}\right)}{\pi \; d_{\text{eq}} L_{\text{h}} \; \text{LMTD}} \tag{7}$$

All fluid properties like density, viscosity, thermal conductivity, and specific heat are evaluated at the average of their values at the simulated mixing cup inlet and outlet temperature.

Fin height

The influence of the fin height on pressure drop and the heat-transfer coefficient was quantified by altering the fin height-to-diameter ratio of the tube, e/D, between zero, that is, a bare tube, and 0.196. Eight fins were adopted in all simulations. For the helicoidally finned tubes, a helix angle of 15.88° was used. The mass-flow rate and the cross-sectional flow area were kept constant, that is, preserving space-time if the gas density at the inlet is constant. It was chosen to keep the minimum metal thickness t fixed to a value of 7.0×10^{-3} m. In practice, this is done for structural stability. This method allows a bare tube with the same equivalent inner diameter to be used as a base case for all finned tubes. The concept is visualized in Figure 4 where the prevalent velocity (A) and temperature (B) fields at the tube outlet are plotted for helicoidally finned tubes with different fin height. The dimensions of the depicted tubes are summarized in Table 1.

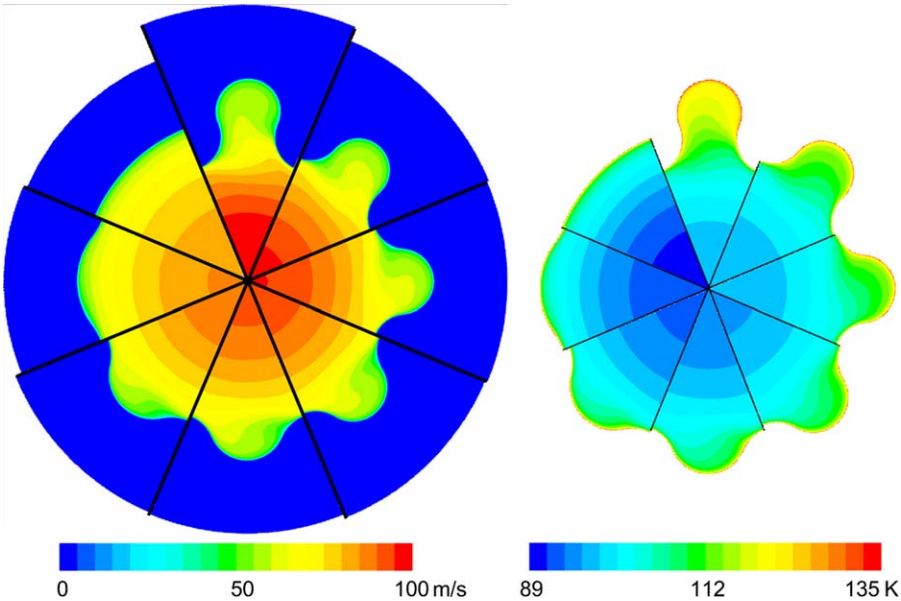

Figure 4. Velocity [m/s] (left) and temperature [K] (right) at the outlet of helicoidally finned tubes with different fin height; clockwise starting at top: F1, F2, F3, F4, F5, F6, F8 and bare, viz. Table 1.

[Color figure can be viewed in the online issue, which is available at wileyonlinelibrary.com.]

Figure 5 shows the heat-transfer coefficient and the pressure drop normalized to the corresponding value of a bare tube as a function of the wetted perimeter. Both types of finned tubes offer substantial improvements in heat transfer. For the longitudinal fins, the heat transfer improvements can be assigned solely to the increase in internal surface area as a linear relationship is observed between the heat-transfer ratio and the wetted perimeter. However, this is not the case for the helicoidally finned tubes. An enhanced cross-sectional mixing can explain the local maximum of the heat-transfer coefficient seen in Figure 5. To quantify this cross-sectional mixing, a dimensionless mixing cup temperature variance in a cross section, Θ_T is introduced

$$\Theta_T = \frac{\sqrt{\frac{\sum\left(\phi_{m,i}\left(T_i - T_{\text{avg}}\right)^2\right)}{\phi_{m,\ \text{tot}}}}}{T_{\text{avg}}} \tag{8}$$

In this equation $\phi_{m,i}$ represents the mass-flow rate through the computational cell i, T_i the temperature of cell i and T_{avg} the mixing cup temperature over all cells of the cross section. Lower values of Θ_T correspond to a more uniform temperature distribution in a cross section. Figure 6 shows this dimensionless mixing-cup averaged temperature variance. For all longitudinally finned tubes a lower uniformity is obtained than for the bare tube. For helicoidally finned tubes, a more uniform cross-sectional temperature profile is obtained at low e/D ratios. Hence, better cross-mixing is established leading to a higher heat-transfer coefficient at low e/D ratios. However, the lowest e/D ratios also offer the smallest increase in internal surface area. The combination of these two opposing effects explains the nonlinear behavior of the heat-transfer coefficient as function of the wetted perimeter ratio for helicoidally finned tubes and that an optimal ratio of fin height-to-diameter exists. The performed simulations for the helicoidal fins indicate this value to be around 0.12. Tubes with an e/D higher than 0.12 will offer additional heating improvements but at the cost of a much higher pressure drop.

Helix angle

Helix angles ranging from 0° (longitudinal fins) to 48° were studied. Two different fin height-to-diameter ratios of 0.037 and 0.147 were studied. Eight fins were adopted in all simulations.

The pressure drop ratio and heat-transfer ratio compared to a bare tube as function of the helix angle are shown in Figure 7. These results indicate that larger helix angles improve heat transfer. Indeed, at higher helix angles swirling flow is induced providing better cross-sectional mixing. As a result of the increased wall shear stresses, also higher pressure drops are simulated. The upper limit of optimal helix angle for the tall fins is in the range between 25 and 30°, because increasing the helix angle further makes the pressure drop increase strongly while gain in heat transfer remains constant. These results correspond with the values proposed by Higuchi et al.[20] for a similar geometry. Alternatively, fins with a reduced height can be used at higher helix angles as they only result in a moderate pressure drop increase.

Table 1. Dimensions of Helicoidally Finned Tubes used in Fin Height Study

Tube ID	F1	F2	F3	F4	F5	F6	F7	F8	Bare
Inner diameter D [10^{-3} m]	39.0	36.8	36.0	35.3	34.6	33.9	33.2	32.6	31.6
Fin height e [10^{-3} m]	7.6	5.4	4.6	3.9	3.2	2.5	1.8	1.2	–
e/D [-]	0.195	0.147	0.128	0.110	0.092	0.074	0.054	0.037	–
Number of fins [-]	8	8	8	8	8	8	8	8	0
Wetted perimeter ratio [-]	1.81	1.44	1.33	1.24	1.16	1.10	1.06	1.02	1.00

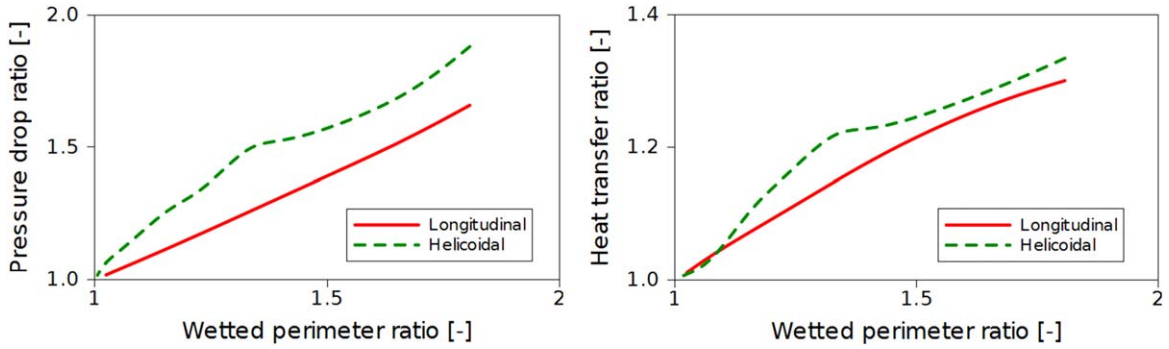

Figure 5. Pressure drop ratio [-] (left) and heat-transfer ratio [-] (right) as function of wetted perimeter ratio [-] for longitudinally finned; — and helicoidally finned; - - - tubes; at $Re = 90 \times 10^3$.

[Color figure can be viewed in the online issue, which is available at wileyonlinelibrary.com.]

Number of fins

Typically between 6 and 12 fins are used in finned steam cracking reactors.[19] The simulation results obtained for an *e/D* ratio of 0.147 with finned tubes containing between 4 and 12 fins are shown in Figure 8. For the helicoidally finned tubes, the helix angle was again 15.88°. A linear relation between the number of fins and pressure drop is observed for both the longitudinally finned and helicoidally finned tubes. However, the heat-transfer ratio increases only up to 8–10 fins. For tubes with more than 10 fins, it was seen that the flow inside the fin valley gets isolated from the tube center leading to lower velocities. As soon as flow isolation inside the fin occurs, an additional heat-transfer resistance emerges due to the narrow passing from the fin valley to the tube center. The simulations illustrate that the optimal number of fins depends strongly on the chosen fin height, which in this case results in an optimal value of 8–10 fins. From these considerations, it can be assumed that the optimal number of fins depends on the fin height, that is, for fins with a small fin height-to-diameter ratio a higher number of fins can be adopted.

Geometry optimization

The parametric study assessed the performance of finned tubes for nonreactive air flow in terms of pressure drop and heat transfer. It allows to formulate several guidelines toward optimal steam cracking reactor design. Ideally low pressure drops are combined with a high radial temperature uniformity, giving rise to high light olefin selectivity and a reduced coking tendency.[49] Hence, based on the results of the preceding parametric study, a design with a small fin height seems potentially attractive because this allows to take maximal advantage of the lower pressure drops these fins induce. In combination with a large value for the helix angle, this could lead to a large increase in heat transfer by swirling flow for a low pressure drop increase. In any case, a clear trade-off between heat-transfer enhancement and additional pressure drop needs to be made. This becomes clear from Figure 9, in which all simulation data points acquired throughout the parametric study are plotted. The relationship between the relative heat transfer and relative pressure drop is highly linear, but it is not obvious to assess the effect on product selectivities and run length based on these data. Translating these guidelines to optimal fin height and number of fins has allowed to define two optimal geometries that should significantly outperform the previously studied tubes. The dimensions of these optimized designs are summarized in Table 2. Geometry "O1" has fins with an *e/D* ratio of 0.11. The helix angle and number of fins were chosen at the optimal values found in the parametric study for the taller fins, that is, 8–10 fins and a helix angle between 25 and 30°. For geometry "O2," 24 small fins are combined with a high helix angle. Both optimized geometries were found to offer increased heating characteristics as seen in Figure 9. Mainly at the highest Reynolds number a better performance is simulated, that is, for a given pressure drop the heat transfer is higher.

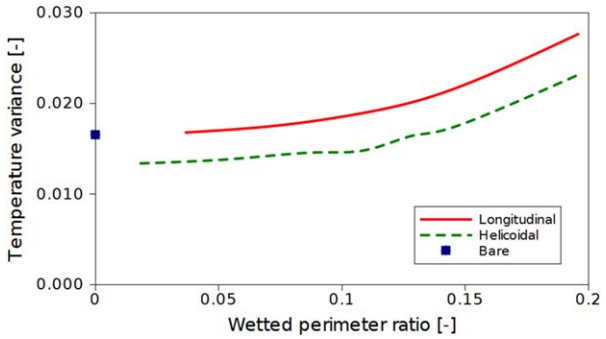

Figure 6. Dimensionless mixing-cup weighted average temperature variance [-], viz. Eq. 8 as function of wetted perimeter ratio [-] for longitudinally finned; — and helicoidally finned; - - - tubes; ■ bare tube.

[Color figure can be viewed in the online issue, which is available at wileyonlinelibrary.com.]

For application in steam cracking reactors, it can be concluded that the optimal geometry will be largely dependent on the process conditions, that is, mainly the Reynolds number. Furthermore, a trade-off between improved heat transfer and increased pressure drop must be made, which depends on the applied feedstock as changes in product selectivity due to the higher pressure drop will differ for different feedstocks.[49] Hence, non-reactive experiments and simulations can offer guidelines for design, but reactive CFD simulations are necessary to assess the actual effect on product yields and coking.

Reactive Simulations of an Industrial Propane Cracker

Reactive simulations of one of the reactors in an industrial Millisecond furnace were performed to assess the effect of

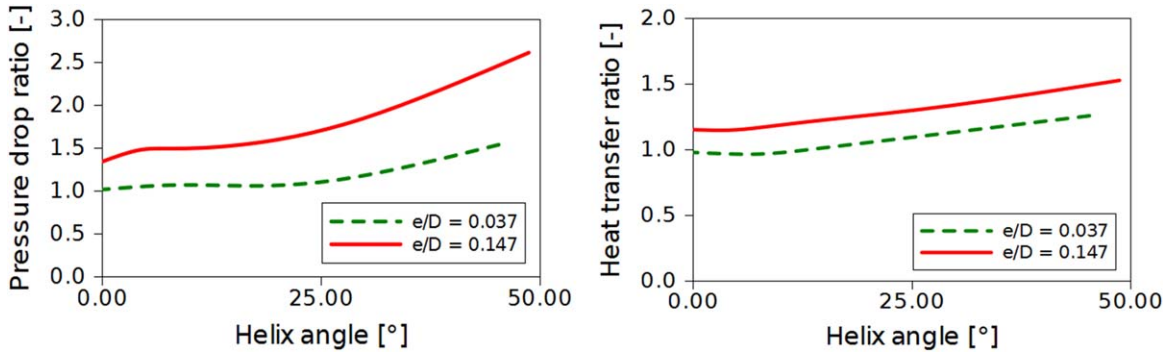

Figure 7. Pressure drop ratio [-] (left) and heat-transfer ratio [-] (right) as function of helix angle [°] for a fin height-to-diameter ratio of 0.037; - - - and a fin height-to-diameter ratio of 0.147; —; at $Re = 90 \times 10^3$.

[Color figure can be viewed in the online issue, which is available at wileyonlinelibrary.com.]

finned reactors on product yields and coking tendency. Millisecond furnaces operate at very high severity and a residence time of approximately 0.1 s. Millisecond furnaces are designed to achieve maximum ethene yield resulting in high operating temperatures and very short run lengths, sometimes as short as one week.

Process conditions and reactor configurations

A 100% pure propane feedstock was adopted. The hydrocarbon and steam flow rate were set to 0.03292 and 0.01075 kg/s, respectively, resulting in a steam dilution 0.33. The reactor inlet temperature was equal to 903.7 K, whereas the reactor outlet pressure, that is, upstream of the transfer line exchanger, was set to be 170 kPa, that is, the industrially applied value.

A coupled reactor-furnace simulation would require iteration between reactor and furnace simulations and is at present impossible due to too high computational cost. Therefore, a heat-flux profile was set as boundary condition on the outer wall of the reactor. This heat-flux profile was taken from a furnace simulation where the boundary condition applied to the outer wall of the reactor tubes was the industrially measured outer wall temperature profile. The adopted models in the furnace simulation were similar to those of Hu et al.[29]

Four different reactor configurations were simulated. Their dimensions are summarized in Table 3. First, a bare tube (Bare) was simulated as a reference case. Second, an industrially applied helicoidally finned reactor (Helix) was considered. The fin dimensions of this reactor are close to those of the optimized geometry "O1," viz. Table 2, of the parametric study. Third, the same fin parameters were applied in simulating a reactor with longitudinal fins (Straight). Finally, a tube with significantly smaller fins was simulated (SmallFins) corresponding to the optimized geometry "O2."

Results and Discussion

The computational grid was constructed by extruding a 2-D mesh of 1/8th of the cross-section applying the required twist vector for the helicoidally finned reactors. The grid size in wall units was maintained at the values used throughout the parametric study which were confirmed to provide grid-independent results. This led to computational grids consisting of 6–11 million cells.

Computation was performed on 32-core Dell C6145 computing nodes with Advanced Micro Devices (AMD) Magny-Cours Opteron 6136 processors and an Infiniband Double QDR communications link. Total CPU time amounted to around 25,000 h per simulation, that is, about 1 month of clock time.

Figures 10A, B show the mixing cup temperature and pressure as function of the axial position for the four reactor configurations. Little differences between the process gas temperature profiles are simulated as the same heat input, reactor volume, and mass-flow rate are adopted. However, the pressure drop varies drastically with SmallFins showing the highest pressure drop. This higher pressure drop results in a higher inlet density yielding small differences in residence time, calculated here as reactor volume divided by volumetric inlet flow rate, as shown in Table 4.

Figure 11 shows the azimuthally area-averaged tube metal skin temperature as function of axial position. The maximum

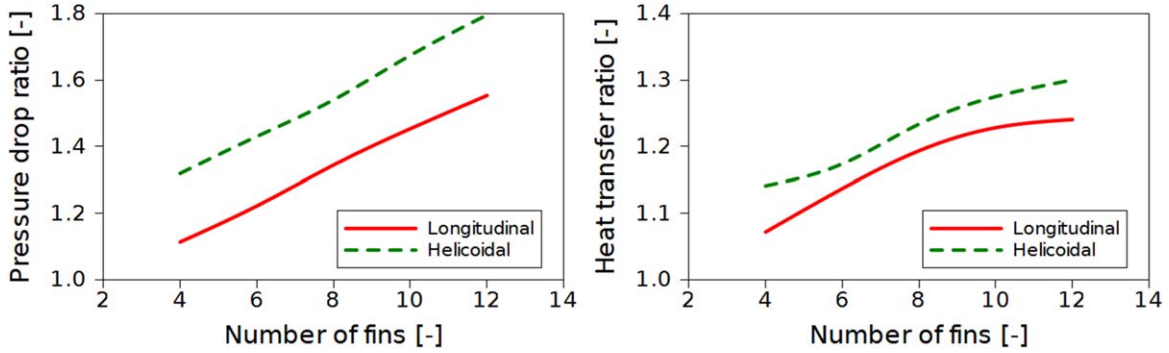

Figure 8. Pressure drop ratio [-] (left) and heat-transfer ratio [-] (right) as function of number of fins [-] for longitudinally finned; — and helicoidally finned; - - - tubes; at $Re = 90 \times 10^3$.

[Color figure can be viewed in the online issue, which is available at wileyonlinelibrary.com.]

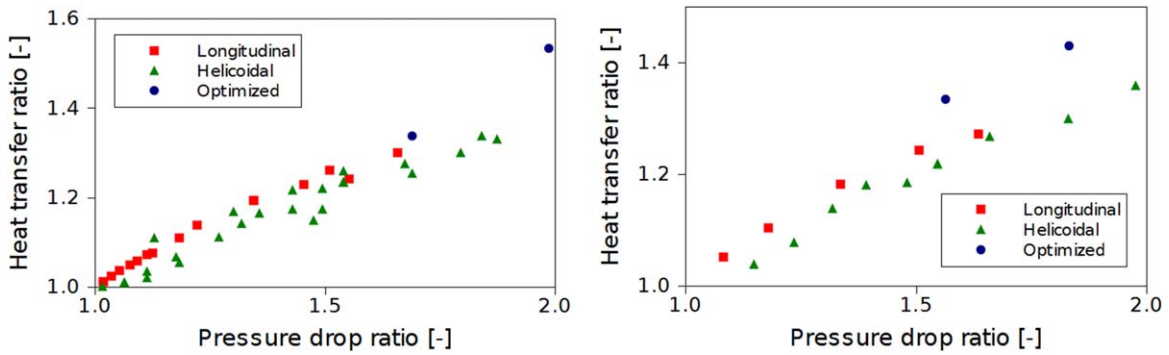

Figure 9. Heat-transfer ratio [-] as function of pressure drop ratio [-] at a Reynolds number of 90 × 10^3 (left) and 130 × 10^3 (right) for longitudinally finned; ■, helicoidally finned; ▲, and optimized; • tubes.

[Color figure can be viewed in the online issue, which is available at wileyonlinelibrary.com.]

TMT occurs at around 3.5 m corresponding to the maximum of the heat flux to the reactor. For the Bare reactor, the maximum temperature is 1334 K, which is close to the maximum allowable TMT of 1363 K. This is because the severity of cracking is very high, that is, the coil outlet temperature (COT) is above 1190 K. The maximum TMT is 29, 26, and 51 K lower than the Bare reactor for Helix, Straight, and SmallFins, respectively. For Millisecond furnaces the maximum tube metal temperature is typically the limiting factor for the run length. Hence, decreasing this temperature by adopting finned tubes will significantly increase the reactor run length.

Table 4 summarizes the most important process conditions, product yields, and selectivities. For validation, data of an industrial bare tube Millisecond reactor running with a crude propane feedstock, that is, 95% pure propane or higher, under similar, but not identical conditions have been added. Considering the accuracy of the industrial yield measurements, the purity of the feed and accounting for the fact that the industrial data are for a slightly lower cracking severity, the agreement between the simulated Bare reactor and the industrial data is reasonable. Comparing the four simulation cases some small differences in COT are observed. These can be attributed to different reaction rates due to different pressure and temperature fields in the four reactors. The coil inlet pressure increases drastically with a factor 1.22 and 1.39 for the Straight and Helix reactor, respectively. As expected from the parametric study, the SmallFins reactor shows the highest pressure drop. The propane conversion is slightly higher for Helix and SmallFins, which can be attributed to a higher space time. To limit the effect of differences in propane conversion, comparison should be made on the basis of selectivities expressed as product yield divided by propane conversion. As bimolecular reactions are favored over monomolecular reactions at higher pressure, the selectivity to light olefins produced by monomolecular beta scissions is reduced at higher reactor pressure. This effect can be clearly seen in Table 4, where the ethene selectivity decreases monotonically with increasing pressure drop ratio. The effect is limited as ethene selectivity only decreases by 0.56 wt %. However, given the large scale of the steam cracking process, this difference is economically significant. The selectivity to methane and 1,3-butadiene is increased as these are formed by a series of bimolecular reaction steps.

Table 2. Dimensions of Optimal Tube Geometries

Tube ID	O1	O2
Inner diameter [10^{-3} m]	35.34	31.32
Fin height [10^{-3} m]	3.89	1.15
Number of fins [-]	10	24
Helix angle [°]	28.7	44.1
Wetted perimeter ratio [-]	1.367	1.212
U ratio [-] for inlet Reynolds number of 90 × 10^3/130 × 10^3	1.31/1.33	1.53/1.43
Pressure drop ratio [-] for inlet Reynolds number of 90 × 10^3/130 × 10^3	1.48/1.56	1.99/1.83

Surprisingly, the SmallFins reactor has the highest propene selectivity although the conversion in this reactor is higher than in all other reactors. Typically the propene yield decreases with increasing conversion.[50] A rate of production analysis of the reaction mechanism reveals that propene is primarily formed by C—H beta scissions of the 2-propyl radical while the addition reaction of the hydrogen radical to propene results in the 1-propyl radical that further decomposes to ethene and methyl

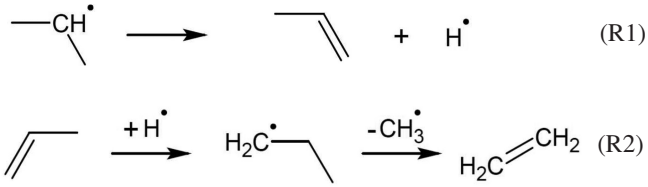

As reported by Van Geem et al.[49] radial temperature gradients strongly affect the radical concentrations and seem to be very likely responsible for the higher propene selectivity. To further assess the effect of conversion on selectivities, a second simulation for the Bare reactor configuration was performed at the same propane conversion of the SmallFins reactor. To this end, the total heat input to the reactor was increased with 0.8%. The results of this simulation are summarized under Bare HighFlux in Table 4. Comparing these results with the SmallFins simulation, it is clear that the reduced ethene selectivity for the SmallFins reactor is completely balanced by the increased selectivity to propene and 1,3-butadiene as the total selectivity to valuable light olefins is almost identical. Hence, application of optimal fin parameters does not necessarily result in a loss of the total olefin selectivity and, for example, during periods where propene and 1,3-butadiene are more valuable than ethene be economically more attractive.

Figure 12A shows the azimuthally mixing-cup averaged process gas temperature as a function of the radial position at an axial position of 10.5 m, that is, near the reactor outlet. As the reactor inner radii vary, the radial position is

Table 3. Reactor Dimensions

Reactor ID	Bare	Helix	Straight	SmallFins
Reactor length [m]	10.556	10.556	10.556	10.556
Adiabatic inlet section [m]	0.444	0.444	0.444	0.444
Maximum inner diameter [10^{-3} m]	30.2	34.8	34.8	31.3
Number of fins [-]	–	8	8	24
Helix angle [°]	–	15.7	–	33.1
Outer diameter [10^{-3} m]	43.7	48.3	48.3	44.8
Metal thickness [10^{-3} m]	6.75	6.75	6.75	6.75
Fin height [10^{-3} m]	–	4.8	4.8	1.15
Cross-sectional surface area [10^{-6} m^2]	715.7	715.7	715.7	715.7
Cross-sectional perimeter [m]	0.0948	0.1315	0.1315	0.1150

normalized. The Bare reactor has a temperature difference between centerline and innerwall equal to 95.6 K. This value is in the same range as reported previously by Van Geem et al.[49] using a 2-D model and De Saegher et al.[19] using a 3-D model, although for different reactors and/or feedstocks. The temperature difference in comparison with Bare is 13.3, 6.9, and 21.4 K lower for the Helix, Straight, and SmallFins, respectively. Due to the lower inner wall temperatures, the finned reactors will yield lower coking rates. The small maximum seen at 0.013 m for Helix and at 0.014 m for SmallFins is a result of a zone with higher temperature in the wake of the fins as was also seen in Figure 4. Figure 12B shows the mixing cup propane yield as function of the radial position at an axial position of 10.5 m. The profiles are normalized to their respective value at the reactor centerline to limit the effect of small differences in conversion. A relative difference of up to 10% is simulated between the center of the reactor and the reactor inner wall for the Bare reactor. Surprisingly, a larger difference of 18% is observed for the Straight reactor. This is attributed to the larger reactor maximum inner diameter compared to the Bare reactor and the absence of enhanced mixing from swirling flow. The better mixing in the Helix reactor reduces the nonuniformity although still not making up completely for the larger reactor inner diameter compared to the Bare reactor. The SmallFins reactor benefits both from better mixing and a lower tube diameter compared to Helix and Straight, yielding the most uniform profile. Figure 12C shows the mixing cup hydrogen radical yield as function of radial position at an axial position of 10.5 m. The profiles are normalized to their respective value at the reactor centerline to limit the effect of small differences in conversion. Comparing these profiles with Figure 12B, it is clear that the hydrogen radical yield shows a much steeper profile close to the reactor wall than the propane yield. This comparison holds for all radicals and molecules. The formation of radicals through C—C and C—H scissions has a high activation energy, whereas the activation energy of radical-consuming recombinations is close to zero. Hence, the formation of radicals is favored at high temperatures. The ranking of radical uniformity between the reactors is, therefore, equal to the ranking of temperature uniformity with Bare being the worst and Smallfins performing best. Taking into account reactions R1 and R2 as determining the propene selectivity, a higher hydrogen concentration near the wall will result in lower propene selectivity as reaction R2 is favored over R1. Higher radial temperature uniformity results in a reduction of propene consuming reactions, leading to a higher propene selectivity.

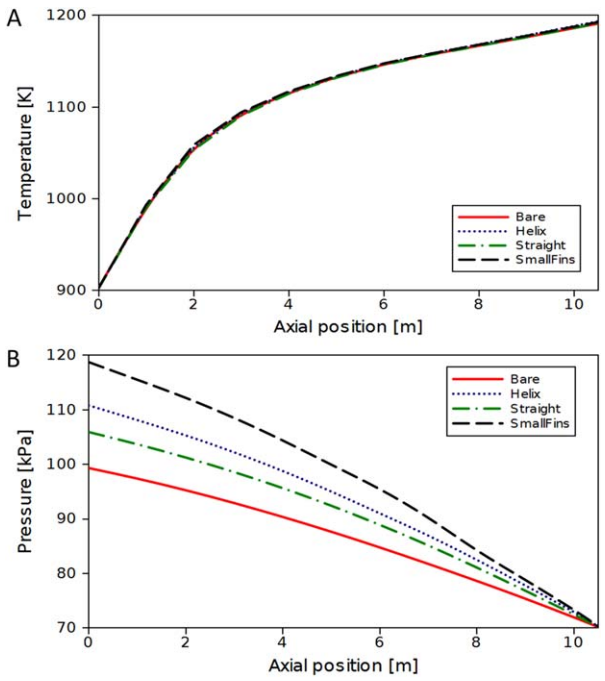

Figure 10. Axial process gas temperature [K] (A) and pressure [kPa] (B) mixing-cup averaged over a cross section as function of axial position [m].

[Color figure can be viewed in the online issue, which is available at wileyonlinelibrary.com.]

Coke formation during steam cracking of hydrocarbons is a complex process. Three distinct mechanisms have been proposed.[51] First, there is a catalytic phase in which the properties of the reactor alloy are important. Afterward, a heterogeneous, noncatalytic, so-called pyrolytic mechanism dominates. Coke can also be formed through a homogeneous noncatalytic mechanism in which high-molecular polyaromatics condensate, collide with the coke surface and get incorporated in the coke layer. In steam cracking reactors, most coke is formed through the pyrolytic mechanism. The modeling of the coke formation is, therefore, focused on the heterogeneous, noncatalytic mechanism.[52] In this mechanism, radical active sites are formed on the coke layer by abstraction reactions by gas-phase radicals followed by additions of gas-phase olefins, terminations by radicals, cyclizations, and dehydrogenation.[53] Hence, the coking rate is determined by the temperature and both molecular and radical gas-phase concentrations near the gas-cokes interface. As the time-scale for coke formation is much smaller than for gas-phase reactions, a discrete approximation can be adopted. This means that coke formation can be assumed constant in a certain time interval, typically 24–48

Table 4. Reactor Conditions, Product Yields, and Selectivities for the Four Reactor Configurations

	Bare	Straight	Helix	Small Fins	Bare High Flux	Bare Industrial[a]
Coil outlet temperature [K]	1190.9	1191.2	1193.5	1192.7	1192.8	–
Pressure drop [kPa]	29.13	35.68	40.49	48.42	28.92	–
Pressure drop ratio [-]	1.00	1.22	1.39	1.66	0.99	–
Propane conversion [-]	84.55	84.74	85.42	85.16	85.20	–
P/E ratio [wt %/wt %]	0.476	0.471	0.471	0.485	0.467	0.50
Residence time [s]	0.149	0.154	0.157	0.163	0.149	–
Product yields [wt %]						
H_2	1.52	1.51	1.51	1.49	1.53	–
CH_4	18.75	19.03	19.22	19.25	18.88	19
C_2H_2	1.03	1.05	1.06	0.98	1.08	–
C_2H_4	38.31	38.39	38.58	38.11	38.67	36
C_2H_6	3.65	3.59	3.58	3.46	3.69	3.5
C_3H_4	1.20	1.24	1.26	1.22	1.25	–
C_3H_6	18.24	18.08	18.17	18.47	18.05	18
C_3H_8	15.45	15.26	14.58	14.84	14.80	17
1,3-C_4H_6	1.23	1.23	1.43	1.53	1.44	1.5
1-C_4H_8	0.54	0.53	0.54	0.56	0.54	–
2-C_4H_8	0.02	0.02	0.03	0.03	0.03	–
n-C_4H_{10}	0.02	0.02	0.02	0.02	0.02	–
Valuable light olefins[b]	57.78	57.70	58.18	58.11	58.15	55
Product selectivities [-]						
H_2	1.80	1.78	1.77	1.75	1.80	–
CH_4	22.18	22.46	22.50	22.61	22.15	–
C_2H_2	1.21	1.24	1.24	1.15	1.27	–
C_2H_4	45.31	45.31	45.16	44.75	45.38	–
C_2H_6	4.31	4.24	4.19	4.07	4.33	–
C_3H_4	1.42	1.47	1.48	1.43	1.47	–
C_3H_6	21.57	21.34	21.27	21.69	21.18	–
1,3-C_4H_6	1.46	1.45	1.67	1.79	1.69	–
1-C_4H_8	0.64	0.62	0.63	0.65	0.63	–
2-C_4H_8	0.03	0.03	0.03	0.03	0.03	–
n-C_4H_{10}	0.02	0.02	0.02	0.02	0.02	–
Valuable light olefins[b]	68.34	68.10	68.10	68.24	68.25	–

[a]Detailed feed composition not available.
[b]Valuable light olefins is the sum of ethene, propene, and 1,3-butadiene.

h is sufficient.[24,54] From the performed simulations, the coking rate at start-of-run conditions, can thus be calculated in a post-processing step from the species concentrations and inner wall temperature.

The semiempirical coking model of Plehiers was used.[54] The parameters in this model were fitted to experimental data using a one-dimensional (1-D) plug flow reactor model and it has shown to give reasonable agreement with both pilot and industrial coking rates.[54] The coking model of Plehiers considers only ethene and propene as coke precursors. Given the typical species concentrations in a propane cracker, these are indeed the main molecules adding to the active radical sites on the coke layer. As the model kinetic parameters were fitted to experimental data using a 1-D model, the mixing cup ethene and propene concentrations are used. However, the kinetic parameter estimation was performed for the coke-gas interface temperature. Hence, the inner wall temperature is used here, rather than the mixing cup gas temperature.

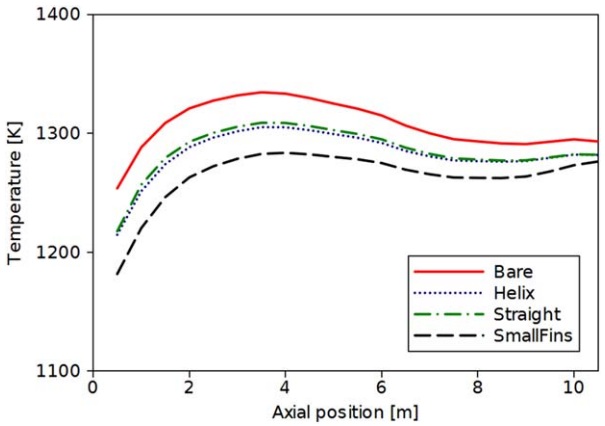

Figure 11. Azimuthally area-averaged tube metal skin temperature [K] as function of axial position [m].

[Color figure can be viewed in the online issue, which is available at wileyonlinelibrary.com.]

Figure 13 shows the azimuthally area-averaged coking rate as function of axial position for the four reactor configurations. All profiles show two maxima; the first around 6 m and the second at the reactor outlet. This shape can be explained by considering the three contributions to the coking rate, that is, the inner wall temperature, the ethene concentration, and the propene concentration. The inner wall temperature shows a similar profile as the outer wall temperature profile shown in Figure 11 having a maximum around an axial position of 4 m. The ethene and propene concentrations are depicted in Figures 14A, B, respectively. The reactors with the highest pressure drop obviously show the highest concentrations due to a higher gas density. The ethene concentration increases monotonically along the reactor. The propene concentration has a maximum at 6 m. Hence, the first maximum in coking rate at 6 m is a result of the temperature and propene concentration maximum. The maximum at the outlet results from the high ethene concentration. Comparing SmallFins to Bare, coking rates are lowered by 48 and 27% at the first and second maximum,

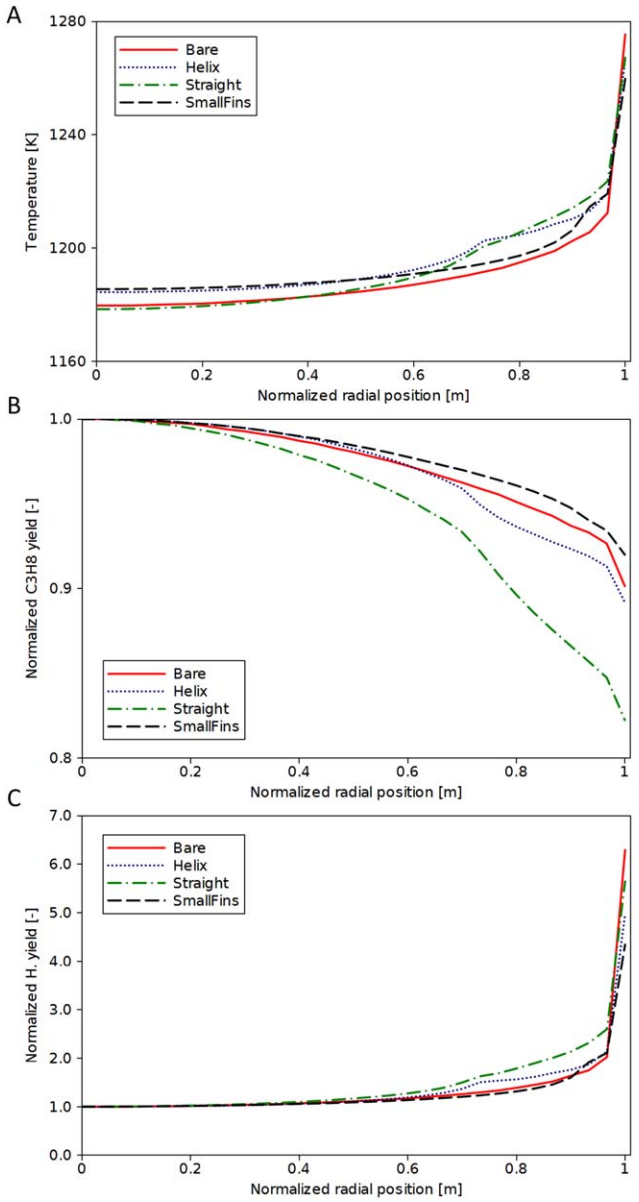

Figure 12. Azimuthally mixing-cup averaged process gas temperature [K] (A), normalized propane yield [wt %/wt %] (B) and normalized hydrogen radical yield [wt %/wt %] (C) as function of radial position at an axial position of 10.5 m.

[Color figure can be viewed in the online issue, which is available at wileyonlinelibrary.com.]

respectively. Hence, run length can be extended greatly by application of finned tubes as a given reduction in the coking rate results in a more than proportional increase of the run length as shown by Wang et al.[5]

Figure 15A shows the coking rate as a function of the relative fin arc length. This relative fin arc length is defined as the running arc length from one fin top to the next divided by the total arc length of one fin. This normalization is necessary as the total fin arc length differs between SmallFins on one side and Helix and Straight on the other. The shape is a direct result of the nonuniform temperature at the reactor inner wall shown in Figure 15B. The average inner wall temperature for the Helix, Straight, and SmallFins reactor

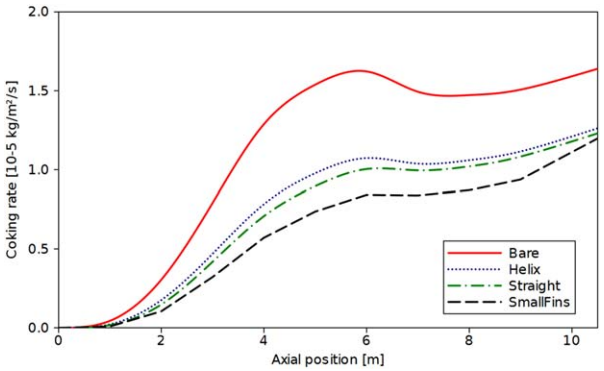

Figure 13. Azimuthally area-averaged coking rate [10^{-5} kg/m^2/s] as a function of axial position [m].

[Color figure can be viewed in the online issue, which is available at wileyonlinelibrary.com.]

are 17.2, 16.8, and 18.5 K lower than the temperature of the Bare reactor. The difference between minimum and maximum temperature is about 15 K for Helix and Straight, whereas it is only 6 K for SmallFins. At a relative fin arc length of 0.11, Helix shows a small local maximum. This is again due to the higher temperature in the wake of the fin also seen in Figure 4. The higher inner wall temperature in the fin valley and resulting higher coke formation will lead to a reduction of the fin height by cokes filling up the fin valleys. This will be most pronounced for the Helix and Straight reactor as the cokes in the fin valley grows about 30% faster compared to the cokes at the fin top. The more uniform temperature profile for SmallFins results in a more uniform growth of the coke layer. Here, the difference in coking rate between fin top and valley is only 10%. Hence,

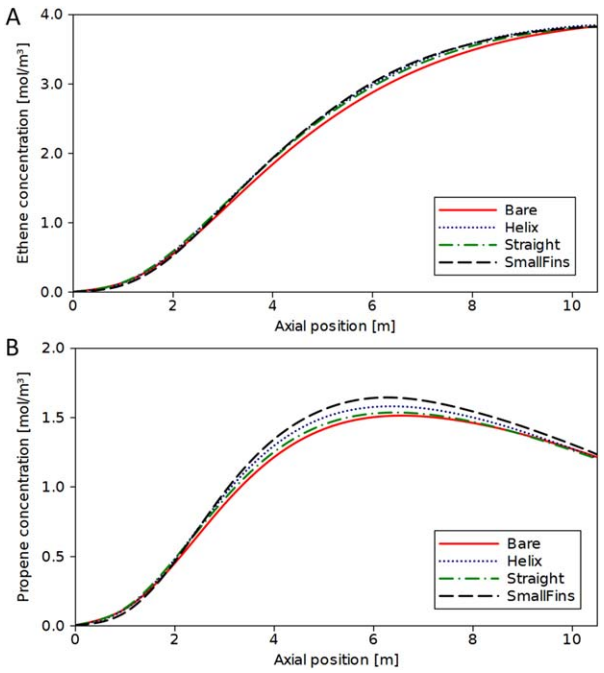

Figure 14. Ethene (A) and propene (B) concentration [mol/m^3] mixing-cup averaged over a cross-section as function of axial position [m].

[Color figure can be viewed in the online issue, which is available at wileyonlinelibrary.com.]

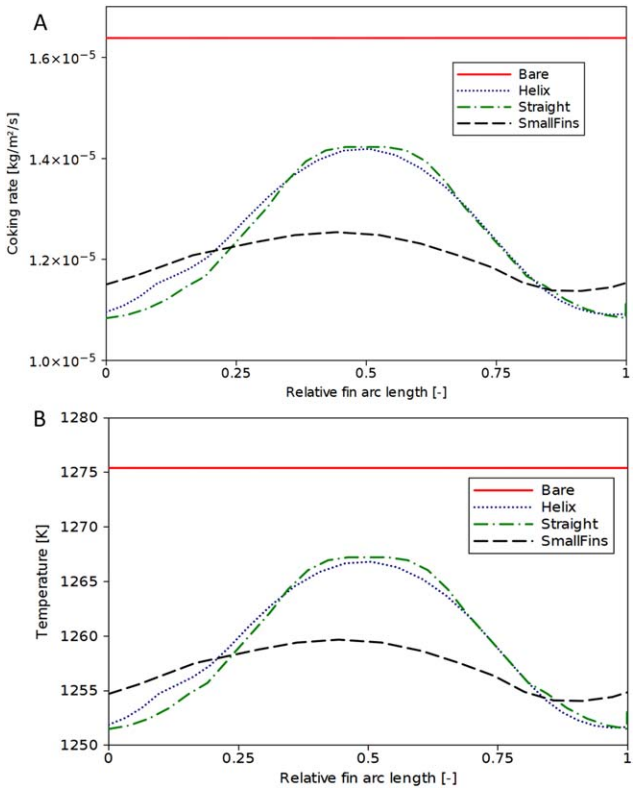

Figure 15. Coking rate [10^{-5} kg/m^2/s] (A) and inner wall temperature [K] (B) as function of the relative fin arc length (0: top; 0.5: valley; 1.0: top) at an axial position of 10.5 m.

[Color figure can be viewed in the online issue, which is available at wileyonlinelibrary.com.]

it is expected that the increased heat transfer due to the finned structure will persist longer for SmallFins. The large nonuniformity of the coking rate shows that azimuthally averaging the coking rate for run length predictions of finned reactors as typically done for bare reactors in 1-D and 2-D reactor models can severely bias the results. For future work, it is, therefore, advised to take the nonuniform buildup of cokes over time into account in order to make realistic run length predictions.

Conclusions

A 3-D reactor model was used for the simulation of internally finned steam cracking reactor tubes. The model agreed well with the experimental validation data of Albano et al.[18] obtained with air. A parametric study optimizing the fin parameters, that is, fin height, helix angle, and number of fins, to maximize heat transfer revealed that the application of small fins with a large helix angle leads to an overall increase in heat transfer for a similar pressure drop. Two optimized designs outperformed all other tube geometries of the parametric study regarding heat transfer. These optimized designs were compared with conventionally used bare reactor tubes for an industrial Millisecond furnace. The reactive simulations with a detailed free-radical reaction mechanism of 203 reactions and 26 species showed that helicoidally finned tubes performed better in comparison to longitudinally finned tubes. Mainly the configuration with 24 small fins and a high helix angle outperformed all other configurations in terms of heat transfer. The corresponding coking rates were found to be 30–50% lower than for the bare tube depending on the fin parameters, which will lead to improved run lengths. However, the large nonuniformity of the coking rates in the azimuthal coordinate could lead to local buildup of cokes over time and could affect the performance. The calculated pressure drop for the finned geometries is significantly higher, especially for the helicoidally finned reactors. It was seen that this can reduce the relative ethene selectivity by more than 1%, whereas it increases selectivity to propene and 1,3-butadiene. An economic trade-off for a specific unit, evaluating the effect of longer run length and shift in light olefin selectivity, should determine the final decision of application of finned reactors. The presented CFD simulations can provide data for such evaluations.

Acknowledgments

CMS acknowledges financial support from a doctoral fellowship from the Fund for Scientific Research Flanders (FWO). The authors also acknowledge the financial support from the Long Term Structural Methusalem Funding by the Flemish Government—grant number BOF09/01M00409. The computational work was carried out using the STEVIN Supercomputer Infrastructure at Ghent University, funded by Ghent University, the Flemish Supercomputer Center (VSC), the Hercules Foundation and the Flemish Government—department EWI.

Notation

Roman

A = tube cross-sectional area, m^2
CFD = computational fluid dynamics
CIP = coil inlet pressure, Pa
COT = coil outlet temperature, K
c_p = heat capacity, J/kg/K
d = diameter, m
e = fin height, m
E = total energy, J
J = diffusional flux, kg/m^2/s
k = turbulent kinetic energy, m^2/s^2
L = axial length, m
LMTD = log-mean temperature difference, K
N = number of fins
nspec = number of species
OD = tube outer diameter, m
p = Pressure, Pa abs
QUICK = quadratic upstream interpolation for convective kinetics
Re = Reynolds number
RNG = renormalization group model
RSM = Reynolds stress model
S = heat of reaction, J/kg/s
T = temperature, K
t = metal thickness, m
TMT = tube skin temperature, K
U = heat-transfer coefficient
u = velocity, m/s
y^+ = dimensionless wall distance
Δy^+ = radial grid spacing in wall units
Y = mass fraction, kg/kg
Δz^+ = axial grid spacing in wall units

Greek letters

ε = turbulent dissipation rate, m^2/s^3
$\Delta\theta^+$ = azimuthal grid spacing in wall units
ρ = density, kg/m^3
ϕ = mass-flow rate, kg/s
τ = stress tensor, Pa

Superscript

t = turbulent

Subscript

eff = effective
h = heat
in = inlet
out = outlet
eq = equivalent, that is, from a disk with the same surface area
abs = absorbed
h = heated
tot = total
avg = mixing cup averaged
m = mass

Literature Cited

1. Ren T, Patel M, Blok K. Olefins from conventional and heavy feedstocks: energy use in steam cracking and alternative processes. *Energy*. 2006;31(4):425–451.
2. Van Geem KM, Marin GB, Hedebouin N, Grootjans J. Energy efficiency of the cold train of an ethylene cracker. *Oil Gas Eur Mag*. 2008;34(2):95–99.
3. Ren T, Patel MK, Blok K. Steam cracking and methane to olefins: energy use, CO2 emissions and production costs. *Energy*. 2008; 33(5):817–833.
4. Van Geem KM, Reyniers MF, Marin GB. Two severity indices for scale-up of steam cracking coils. *Ind Eng Chem Res*. 2005;44(10): 3402–3411.
5. Wang JD, Reyniers MF, Van Geem KM, Marin GB. Influence of silicon and silicon/sulfur-containing additives on coke formation during steam cracking of hydrocarbons. *Ind Eng Chem Res*. 2008;47(5):1468–1482.
6. Wang JD, Reyniers MF, Marin GB. Influence of dimethyl disulfide on coke formation during steam cracking of hydrocarbons. *Ind Eng Chem Res*. 2007;46:15.
7. Reyniers M-F, Froment GF. Influence of metal-surface and sulfur addition on coke deposition in the thermal-cracking of hydrocarbons. *Ind Eng Chem Res*. 1995;34(3):773–785.
8. Parks SB, Schillmoller CM. Use alloys to improve ethylene production. *Hydrocarbon Process*. 1996;75(3):53–60.
9. Redmond T, Bergeron MP. Tests demonstrate anticoking capability of new coating. *Oil Gas J*. 1999;97(19):39–42.
10. Albright LF, McGill WA. Aluminized ethylene furnace tubes extend operating life. *Oil Gas J*. 1987;85(35):46–50.
11. Broutin P, Ropital F, Reyniers MF, Froment GF. Anticoking coatings for high temperature petrochemical reactors. *Oil Gas Sci Technol-Revue d'IFP Energies Nouvelles*. 1999;54(3):375–385.
12. Ganser A, Wynns KA, Kurlekar A. Operational experience with diffusion coatings on steam cracker tubes. *Mater Corros-Werkst Korros*. 1999;50(12):700–705.
13. Ravigururajan TS, Bergles AE. Development and verification of general correlations for pressure drop and heat transfer in single-phase turbulent flow in enhanced tubes. *Exp Therm Fluid Sci*. 1996;13(1):55–70.
14. Jensen MK, Vlakancic A. Experimental investigation of turbulent heat transfer and fluid flow in internally finned tubes. *Int J Heat Mass Transf*. 1999;42(7):1343–1351.
15. Zdaniuk GJ, Chamra LM, Mago PJ. Experimental determination of heat transfer and friction in helically-finned tubes. *Exp Therm Fluid Sci*. 2008;32:15.
16. Ravigururajan TS, Bergles AE. Visualization of flow phenomena near enhanced surfaces. *J Heat Transf*. 1994;116(1):54–57.
17. Brown DJ. Internally finned radiant coils: a valuable tool for improving ethylene plant economics. *6th EMEA Petrochemicals Technology Conference*. London, UK, 2004.
18. Albano JV, Sundaram KM, Maddock MJ. Applications of extended surfaces in pyrolysis coils. *Energy Prog*. 1988;8(3):9.
19. De Saegher JJ, Detemmerman T, Froment GF. Three dimensional simulation of high severity internally finned cracking coils for olefins production. *Oil Gas Sci Technol-Revue de l'Institut Francais du Petrole*. 1996;51(2):245–260.
20. Higuchi J, Hamaogi K, Inventors. Sumitomo Metal Industries, Ltd., assignee. Metal tube for pyrolysis reaction. US patent 8,114,355 B22009.
21. Wolpert P, Ganser B, Jakobi D, Kirchheiner R, Inventors. Schmidt + Clemens Gmbh + Co. Kg, assignee. Process and finned tube for the thermal cracking of hydrocarbons. US patent 20050131263 A12005.
22. Stefanidis GD, Van Geem KM, Heynderickx GJ, Marin GB. Evaluation of high-emissivity coatings in steam cracking furnaces using a non-grey gas radiation model. *Chem Eng J*. 2008;137(2):411–421.
23. Stefanidis GD, Merci B, Heynderickx GJ, Marin GB. Gray/nongray gas radiation modeling in steam cracker CFD calculations. *AIChE J*. 2007;53(7):1658–1669.
24. Heynderickx GJ, Froment GF. Simulation and comparison of the run length of an ethane cracking furnace with reactor tubes of circular and elliptical cross sections. *Ind Eng Chem Res*. 1998;37(3):914–922.
25. Habibi A, Merci B, Heynderickx GJ. Multiscale modeling of turbulent combustion and NOx emission in steam crackers. *AIChE J*. 2007;53(9):2384–2398.
26. Habibi A, Merci B, Heynderickx GJ. Impact of radiation models in CFD simulations of steam cracking furnaces. *Comput Chem Eng*. 2007;31(11):1389–1406.
27. Hu G, Wang H, Qian F, Zhang Y, Li J, Van Geem KM, Marin GB. Comprehensive CFD simulation of product yields and coking rates for a floor- and wall-fired naphtha cracking furnace. *Ind Eng Chem Res*. 2011;50(24):13672–13685.
28. Hu G, Wang H, Qian F. Numerical simulation on flow, combustion and heat transfer of ethylene cracking furnaces. *Chem Eng Sci*. 2011;66(8):1600–1611.
29. Hu G, Wang H, Feng Q, Van Geem KM, Schietekat CM, Marin GB. Coupled simulation of an industrial naphtha cracking furnace equipped with long-flame and radiation burners. *Comput Chem Eng*. 2012;38:24–34.
30. Tang Q, Denison M, Adams B, Brown D. Towards comprehensive computational fluid dynamics modeling of pyrolysis furnaces with next generation low-NO(x) burners using finite-rate chemistry. *Proc Combust Inst*. 2009;32:2649–2657.
31. Lan X, Gao J, Xu C, Zhang H. Numerical simulation of transfer and reaction processes in ethylene furnaces. *Chem Eng Res Des*. 2007; 85(A12):1565–1579.
32. Sabbe MK, Van Geem KM, Reyniers M-F, Marin GB. First principle-based simulation of ethane steam cracking. *AIChE J*. 2011; 57(2):482–496.
33. Sun W, Saeys M. Construction of an ab initio kinetic model for industrial ethane pyrolysis. *AIChE J*. 2011;57(9):2458–2471.
34. Van Geem KM, Reyniers MF, Marin GB, Song J, Green WH, Matheu DM. Automatic reaction network generation using RMG for steam cracking of n-hexane. *AIChE J*. 2006;52(2):718–730.
35. Ranzi E, Frassoldati A, Granata S, Faravelli T. Wide-range kinetic modeling study of the pyrolysis, partial oxidation, and combustion of heavy n-alkanes. *Ind Eng Chem Res*. 2005;44(14):5170–5183.
36. Pitz WJ, Mueller CJ. Recent progress in the development of diesel surrogate fuels. *Prog Energy Combust Sci*. 2011;37(3):330–350.
37. Clymans PJ, Froment GF. Computer-generation of reaction paths and rate-equations in the thermal cracking of normal and branched paraffins. *Comput Chem Eng*. 1984;8(2):137–142.
38. Van Geem KM, Hudebine D, Reyniers M-F, Wahl F, Verstraete JJ, Marin GB. Molecular reconstruction of naphtha steam cracking feedstocks based on commercial indices. *Comput Chem Eng*. 2007;31(9): 1020–1034.
39. Van Geem KM, Zajdlik R, Reyniers M-F, Marin GB. Dimensional analysis for scaling up and down steam cracking coils. *Chem Eng J*. 2007;134(1–3):3–10.
40. Green WH, Allen JW, Bhoorasingh P, Buesser BA, Ashcraft RW, Beran GJ, Class CA, Gao C, Goldsmith CF, Harper MR, Jalan A, Khanshan FS, Magoon GR, Matheu DM, Merchant SS, Mo JD, Petway S, Raman S, Sharma S, Slakman B, Song J, Geem KMV, Wen J, West RH, Wong A, Wong H-W, Yelvington PE, Yee N, Yu J. Reaction Mechanism Generator, 2013, http://rmg.mit.edu/.
41. Jones JE. On the determination of molecular fields. I. From the variation of the viscosity of a gas with temperature. *Proc R Soc London Ser A*. 1924;106(738):441–462.
42. Bird RB, Stewart WE, Lightfoot EN. Transport Phenomena. New York, NY, US: Wiley, 2006.
43. Lemmon EW, Jacobsen RT. Viscosity and thermal conductivity equations for nitrogen, oxygen, argon, and air. *Int J Thermophys*. 2004;25:21–69.
44. McGee HA. Molecular Engineering. New York: McGraw-Hill, 1991.
45. Kuo KKY. Principles of Combustion. New York: Wiley-Interscience, 2005.
46. Leonard BP. Order of accuracy of QUICK and related convection-diffusion schemes. *Appl Math Model*. 1995;19(11):640–653.

47. Andersson B, Andersson R, Hakansson L, Mortensen M, Sudiyo R, van Wachem B. *Computational Fluid Dynamics for Engineers, 7th ed*. Cambridge, UK: Cambridge University Press, 2012.
48. Von Kármán T. *Mechanical Similitude and Turbulence*. Washington DC: National Advisory Committee for Aeronautics, 1931.
49. Van Geem KM, Heynderickx GJ, Marin GB. Effect of radial temperature profiles on yields in steam cracking. *AIChE J*. 2004;50(1):173–183.
50. Froment GF. Kinetics and reactor design in the thermal-cracking for olefins production. *Chem Eng Sci*. 1992;47(9–11):2163–2177.
51. Wauters S, Marin GB. Kinetic modeling of coke formation during steam cracking. *Ind Eng Chem Res*. 2002;41(10):2379–2391.
52. Wauters S, Marin GB. Computer generation of a network of elementary steps for coke formation during the thermal cracking of hydrocarbons. *Chem Eng J*. 2001;82(1–3):267–279.
53. Reyniers GC, Froment GF, Kopinke FD, Zimmermann G. Coke formation in the thermal cracking of hydrocarbons. 4. Modeling of coke formation in naphtha cracking. *Ind Eng Chem Res*. 1994;33(11):2584–2590.
54. Plehiers PM, Reyniers GC, Froment GF. Simulation of the run length of an ethane cracking furnace. *Ind Eng Chem Res*. 1990;29(4):636–641.

Manuscript received Aug. 13, 2013, and revision received Dec. 6, 2013.